International Journal of
INTELLIGENT SYSTEMS AND APPLICATIONS IN ENGINEERING
ISSN:2147-6799 www.ijisae.org Original Research Paper

# Abnormality Classification in PET Images of Prostate Tumour using Neural Network Methods

**Dr. Prabha Ravi[1], Dr. C. K. Narayanappa[1], Dr. Nandeesh M. D.[1], Nayana Bangaru[1], Deepthi Nandha[1], Pavana D. S. [1]**

**Submitted:** 07/09/2023 **Revised:** 21/10/2023 **Accepted:** 04/11/2023

**Abstract:** The second most commonly affecting disease among males across the world is prostate cancer. The occurrence of prostate cancer has shown significant variation across the world. Many countries have done extensive study on the distribution of the disease and its characteristics to find the vital parameters and methods that could enable timely and precise diagnosis and therapy.Thisincludes the analysis of information obtained from different methods in decision making. Most commonly blood tests to find PSA levels is the primary test which is generally followed by MRI guided biopsies. In this study, application of computer aided diagnostic method is implemented and the outcomes are analysed with the intention that the use of AI would reduce the subjectivity of the findings at large. Use of Artificial Intelligence in cancer diagnosis help for early diagnosis, treatment and monitoring enabling remote access to experts. Functional imaging techniques when combined with CT or MRI scans should facilitate quick diagnosis times to allow for rapid response and treatment. However, positron emission tomography, when used for prostate cancer imaging, still relies on manual contour drawing and feature extraction to pinpoint tumour location. This process can take up to several days.

In this paper, an attempt has been made to streamlinethe process by performing automated tumour location pinpointing using image processing techniques. We have also used machine learning techniques and compared the results to automatically diagnose the tumour as benign or malignant. The back propagation method, Support Vector Machine approach and Convoluted Neural network models have been performed.

The automated process with specialist oversight may allow and enable faster response time and more effective treatment enabling computer assisted diagnostic approach facilitating both the qualitative and quantitative aspects.

***Keywords***: *PET, Prostrate, cancer, medical image,machine learning, convolutional neural networks.*

## 1. Introduction

The second most frequent cancer to affect men is prostate cancer [1]. In the year 2020, the number of new cases of prostate cancer globally was 1,414,259 which caused 375,304 deaths. Prostate cancer comprises of more than 7% of all cancers cases and it is the most diagnosed malignancy in males in 112 countries. The risk of cancer increases significantly after the age of sixty[2]. Prostate cancer is a slow progressive cancer and the small tumors can be not easy to detect. Early diagnosis is through a digital rectal exam where a physician is able to feel the back of the prostate gland for any nodules present. The presence of prostate-specific antigen (PSA) in the blood is also tested. However, prostate cancer sometimes does not exhibit elevated levels of PSA [3]. Hence, this type of diagnosis is sometimes faulty,and a biopsy is required for confirmation[4]. Various imaging methods are used to determine the spread of the cancer like PET, MRI, Ultrasound, etc. Positron emission tomography (PET) scanning images the functional activity of the body and its organs.

A short-lived radioactive isotope (fluorodeoxyglucose (FDG)) is used as a tracer which gets metabolized by the body [5][9]. The tracer appears concentrated wherever the body displays high cellular or metabolic activity. Abnormal spots of activity in the scan usually indicate disease, namely cancerous activity. These areas of high activity are revealed as bright spots on a PET scan.

PET scans tend to be blurry and lack comprehensive anatomical information since they are used only for functional activity imaging. A CT scan or an MRI scan, on the other hand, has detailed anatomical information. Combining both yields a scan that has sufficient information for a clinician to locate the area of disease [6]. Using a PET scan, a physician has to manually extract the region of interest which is time-consuming and erroneous. Benign and malignant tumors are difficult to discern. An efficient automated method to detect, draw boundaries and classify tumours from PET scans was required[7].

[1] *Ramaiah Institute of Technology, Bangalore, India*
*prabharavi@msrit.edu , c_k_narayanappa@msrit.edu , mdnandeesh@msrit.edu*

## 2. Literature Review

Standard Uptake Value (SUV) gives the measurement of the tracer uptake in a lesion normalized to a distribution volume, which has been a predominantly considered factor to determine if a region is malignant or benign. Understanding of Multi-modal imaging in evaluation of tumor response to therapy and accurately identifying the diseased region with high resolution is considered.

Clinical utility of 18F Choline instead of Fluoro-deoxy-glucose (FDG) for imaging the metastasis staging of high-risk prostate cancer was observed.

Segmentation methods used to obtain the Region of Interest (ROI) were Otsu's thresholding, graph-based co-segmentation, and active contour methods which required manual specification of the threshold value through the histogram analysis. Hence, the need for automated segmentation and classification of the tumor based on various parameters was observed [8][10].

Requirements are :

- PET images [28].
- MATLAB Software Tool

## 3. Methodology

**3.1 Overview:** The methodology involved:

1. Identifying open-source PET images and PET images from hospital.
2. Manual classification of PET images.
3. Segmentation and feature extraction of PET images
4. Automated classification using Back propagation support vector machine & convolutional neural network models.
5. 3D Model reconstruction
6. Development of Graphical User Interface for computer aided diagnosis(CAD).
7. Pseudo coloured Image of ROI

The RGB image is first converted to Gray scale image. The conversion is for the advantage of having only one image layer of 0 to 255. The complexity of the processing technique is simplified. Thus, obtained threshold values of the Grayscale image is processed for feature extraction. The mean, standard deviation ,entropy , region of interest and area were the features considered along with standard uptake value and decay factor which are vital parameters in nuclear imaging .With these feature values obtained , the three methods namely ,back propagation method ,support vector machine model and convolutional neural network model-based classification is obtained. Finally, the analysis of the classification were carried out subjecting to receiver operating characteristics curve, confusion matrix an d accuracy of the three methods.

The edge detection using Sobel mask is done and then pseudo color image processing was executed. This step was with the intention to provide visual clarity of the abnormality boundaries. The inclusion of 3D reconstruction was implemented and displayed along with that of the graphical user interface is to enhance the visual perception of the abnormality region.

Steps Involved in the proposed methodology is schematically represented in figure 3.1 in order comprehend the connectivity of each step involved in the process. It shows the flow of work planned and executed. The radiation pulses count number is obtained by the computer during a preset time periodwas presented in the video screen as a spot. Its intensity is displayed in shades of Gray. Black represents no activity (zero counts) and white indicates the maximum count level [11].

**3.2 Dataset:** About 900 slices of PET images on prostate cancer was used from open data set to train and test the working of algorithms. The archived patient data set obtained from the hospital was considered as input data set for classification. An archived PET dataset of 10 patients was used for implementation. The dataset included 619 slices of each patient with the tumor cells present in some of them. The patients received an intravenous (IV) radioactive antibody injection on the first day. Imaging took place in two sessions, 24 or more hours apart. Here the images were carefully screened for selecting the slices of the prostrate area as ROI , if the patient data is a whole body scan.

**3.3 Implementation**

The methods used to segment the region of interest were negative transformation, contrast stretching and thresholding. Segmentation was followed by feature extraction. Features such as mean, standard deviation, region of interest, area, entropy, standard uptake value, decay factor, highest pixel intensity and lowest pixel intensity were extracted [12][13].

P value and box plots were plotted to distinguish between benign and malignant groups. Classification was carried out using back propagation and support vector machine.

Receiver operating characteristic curve and confusion matrix are plotted. A convolutional neural network (AlexNet) was implemented for automated classification.3D reconstruction was carried out using the Volume Viewer. Rendering editor component was used to isolate the structures of interest and to make other layers transparent. Finally, using various heat maps, the data was viewed as an isosurface or a maximum intensity projection [14].

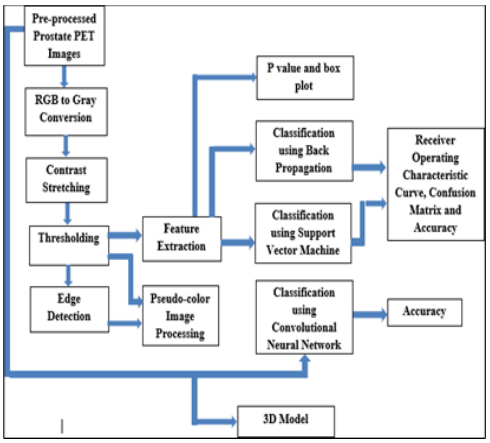


**Fig: 3.1** Schematic Representation

### *3.3.1 Step 1: Segmentation*

PET scans are RGB images. To reduce the amount of data present in the image and for easier processing, the image is converted to grayscale [15]

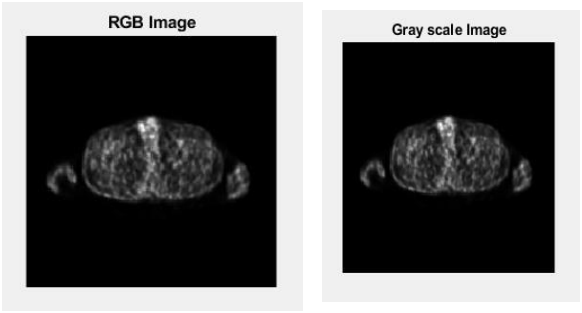


**Fig 3.2**: RGB Image & its Gray

To detect the boundary of the tumor and separate it from the background of the image, segmentation was implemented [16][17].The image was first negatively transformed before any further processing to clearly demark the only light tumor area in the dark image. The output image was obtained by subtracting each value of the input image from the highest Gray level present. The resulting image helped in identifying the darker regions of highest SUV uptake value indicating a region of interest [18].

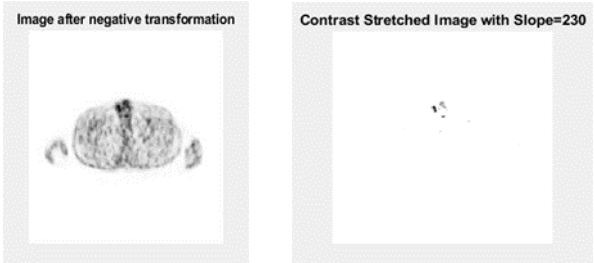


**Fig 3.3** Negative transform & contrast stretched image

To further increase the contrast of the image and make the region clearer, the original Gray levels were stretched linearly taking the histogram as reference. Low intensity pixels were retained [22].

The mathematical representation can be shown as:

$$g(f) = af + b$$

Where:

g is the image after contrast stretching
f is the input Gray scale image
a is the slope
b is the intercept

The histogram of the original PET image was studied and any value above 150 was made to be 65535 using a slope of 203 and an intercept of 0. Low intensity pixels were retained [19] [20].ROI is selected. Thresholding-based PET image segmentation was performed to obtain the highest uptake region, which is usually smaller than the background areas. Since all the high intensity levels were made 65535 in the previous step, the threshold was kept as maximum Gray level-1 (65534).

For any grayscale value above or equal to the threshold value, the pixel was changed to white. Anything below the threshold value, it was made to be 0 to obtain a binary image.

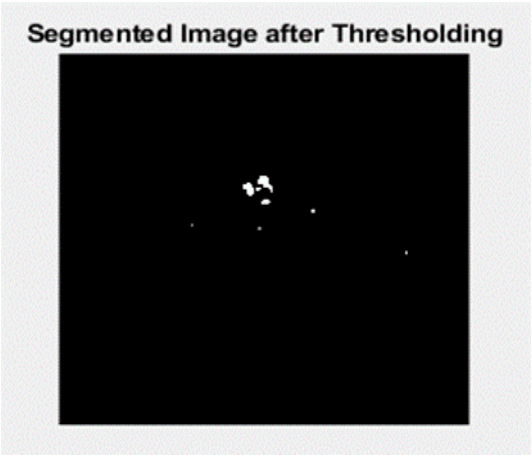


**Fig 3.4:** Segmented & Thresholded Image


**Fig 3.5:** Edge Detection of the Segmented Image

Since a boundary of the tumor was needed, the pixel wise gradients in the smoothened image were calculated by applying the Sobel operator. The gradient in the x and y

direction was approximated by applying the Sobel operator kernels [21].
Sobel horizontal operator is given by:

$$G_X = \begin{bmatrix} -1 & -2 & -1 \\ 0 & 0 & 0 \\ 1 & 2 & 1 \end{bmatrix}$$

Sobel vertical operator is given by:

$$G_Y = \begin{bmatrix} -1 & 0 & 1 \\ -2 & 0 & 2 \\ -1 & 0 & 1 \end{bmatrix}$$

2D convolution operation was carried out and the response was maximum where a line is detected [23].
For better visualisation of the tumor, pseudo-color image processing was used. All the Gray levels with intensity 1 were changed to red. Finally the result of the segmentation procedure shows a red area, indicating the tumor.
Color is assigned for the pixels in the resultant image. It is done based on the plane-by-plane basis. Best intensity slicing is when slicing is done based on physical characteristics.

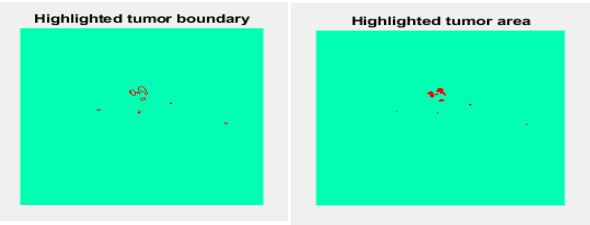


**Fig 3.6:** Highlighted Tumor Area & Highlighted Tumuor Boundary

### *3.3.2 Step 2: Feature Extraction*

Step 1 processing and segmentation was carried on both the benign and malignant tumour image datasets. The following statistical feature values along with SUV were obtained to differentiate between the two datasets. The statistical values obtained for the abnormal area with respect to benign and malignant were significantly varying and so was the SUV , which showed that these selected features were able to differentiate the abnormality as benign and malignant.

**Table: 3.1**

| FEATURE | BENIGN | MALIGNANT |
|---|---|---|
| Entropy(J/K)) | 0.746234 | 0.874148 |
| Mean | 22.0565 | 30.56088 |
| Standard Deviation | 65.368 | 86.31342 |
| Region of Interest | 430350 | 10289100 |
| Area(sq.cm) | 0.008112 | 0.146692 |
| SUV (kBq/mL) | 0.201394 | 4.815069 |
| Decay Factor($s^{-1}$) | 1.14799 | 1.1403 |
| Highest Pixel Intensity | 840 | 943 |
| Lowest Pixel Intensity | 0 | 0 |

The area gave us the extent of the tumor in sq. cm.
It was given by the formula:

Area = {Region of Interest (ROI) x 0.026 x 0.026}

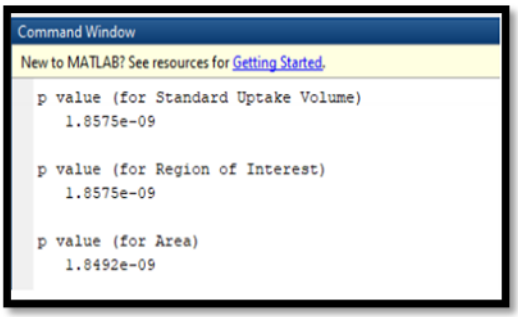


**Fig: 3.7:** P value for SUV


**Fig 3.8** Confusion Matrix using BP

SUV (standard uptake value) is a semiquantitative measure of tracer uptake by the abnormal cells and volume of distribution. As was expected, the SUV of malignant tumors was much more than benign tumors given the difference in ROI [24].
It is given by,
SUV = ROI / (Injected Dose/Patient weight)
The p-value was found to be 1.8267x10-4.

Box plots of the SUV for the two different sets of data were also drawn which showed a significant difference between benign and malignant tumours.

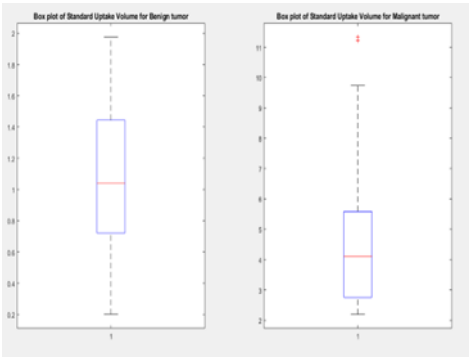


**Fig 3.9** Box plot

For the next step of automatically classifying images for physicians, these features were used with greater weight given to the SUV parameter.

### *3.3.3: Step 3: Classification*

Using the features extracted from the processed images of both datasets, various neural networks were applied for classification. They are discussed as follows: Back Propagation, Support Vector Machine and Convolutional Neural Networks model.

BACKPROPAGATION

Various methods were used for classification. Using backpropagation, the weights associated with the input layer and the hidden layer were adjusted every iterative round in relation to the error produced.

The schematic diagram of confusion matrix and ROC for this classification are as shown below:

Confusion matrix: It is used to describe the performance of a classification model on a set of test data for which the true values are known.

Receiver Operating Characteristic Curves:

"Receiver Operating Characteristics" function (ROC function)is a measure of the performance of a binary classifier.

The curve gives the rate of true positives as a function of the false positive rate and shows the progress made with a binary classifier when the discrimination threshold varies.

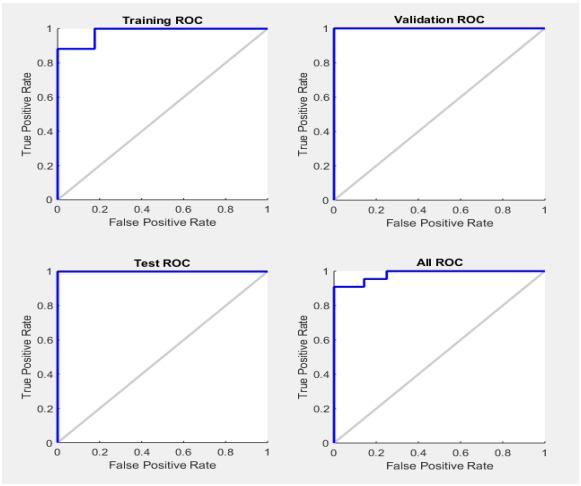


**Fig 3.10:** ROC Curve using Back Propagation

SUPPORT VECTOR MACHINE

SVM is a binary classifier that finds the best hyperplane to separate all data points of one class from those of the other class.

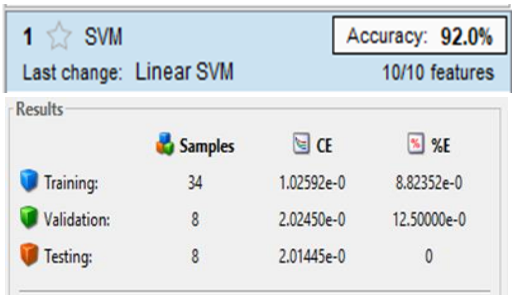


**Fig 3.11:** Accuracy of SVM

Scatterplots were useful for interpreting trends in the statistical data.

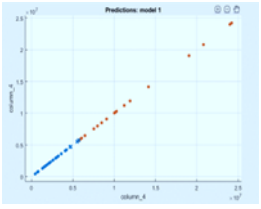

**Fig 3.12:** Scatter Plot

A confusion matrix used here is describes the performance of a classification model on a set of test data for which the true values are known [25].

ROC for this type of classification is shown below in figure 3.13. The accuracy for this type of classification was recorded as 92%.

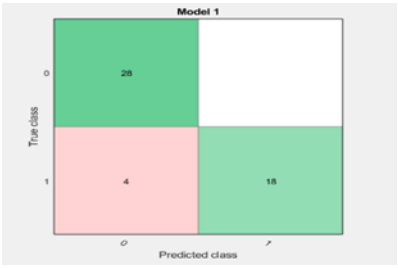


**Fig 3.13** confusion matrix

CONVOLUTIONAL NEURAL NETWORK

AlexNet is one of the deep ConvNets designed to deal with complex scene classification tasks on Imagenet data. A real time plotting of the curve on accuracy and loss in the classified dataset is observed. Accuracy obtained was 87.5 %. [26].

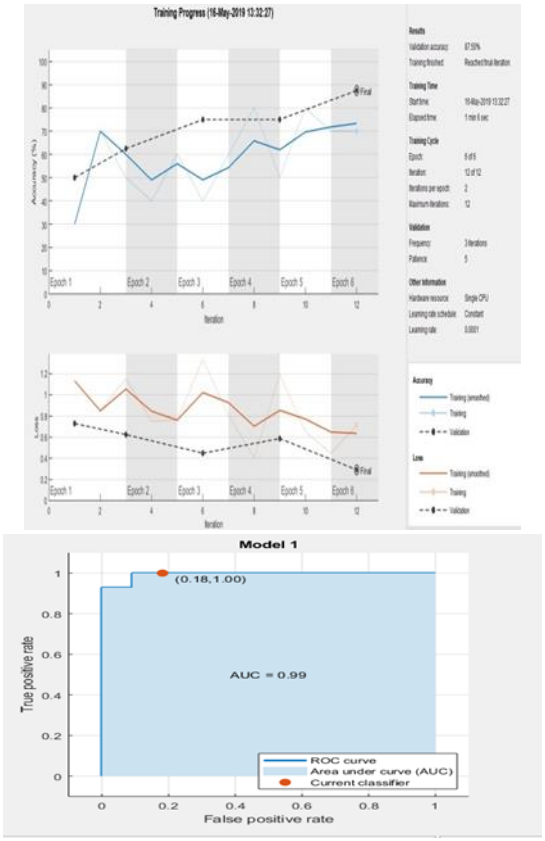


**Fig 3.14 (a):** Results of CNN

```
layers =

  25x1 Layer array with layers:

     1   'data'    Image Input                 227x227x3 images with 'zerocenter' normalization
     2   'conv1'   Convolution                 96 11x11x3 convolutions with stride [4  4] and padding [0  0  0  0]
     3   'relu1'   ReLU                        ReLU
     4   'norm1'   Cross Channel Normalization cross channel normalization with 5 channels per element
     5   'pool1'   Max Pooling                 3x3 max pooling with stride [2  2] and padding [0  0  0  0]
     6   'conv2'   Convolution                 256 5x5x48 convolutions with stride [1  1] and padding [2  2  2  2]
     7   'relu2'   ReLU                        ReLU
     8   'norm2'   Cross Channel Normalization cross channel normalization with 5 channels per element
     9   'pool2'   Max Pooling                 3x3 max pooling with stride [2  2] and padding [0  0  0  0]
    10   'conv3'   Convolution                 384 3x3x256 convolutions with stride [1  1] and padding [1  1  1  1]
    11   'relu3'   ReLU                        ReLU
    12   'conv4'   Convolution                 384 3x3x192 convolutions with stride [1  1] and padding [1  1  1  1]
    13   'relu4'   ReLU                        ReLU
    14   'conv5'   Convolution                 256 3x3x192 convolutions with stride [1  1] and padding [1  1  1  1]
    15   'relu5'   ReLU                        ReLU
    16   'pool5'   Max Pooling                 3x3 max pooling with stride [2  2] and padding [0  0  0  0]
    17   'fc6'     Fully Connected             4096 fully connected layer
    18   'relu6'   ReLU                        ReLU
    19   'drop6'   Dropout                     50% dropout
    20   'fc7'     Fully Connected             4096 fully connected layer
    21   'relu7'   ReLU                        ReLU
    22   'drop7'   Dropout                     50% dropout
    23   ''        Fully Connected             2 fully connected layer
    24   ''        Softmax                     softmax
    25   ''        Classification Output       crossentropyex

accuracy =

    0.8750
```

**Fig 3.14 (b):** Results of CNN

### *3.1.4: Step 4: 3d Reconstruction*

It obtains the localized coordinates of the tumor and the color coded model aids with better visual perception of the cancer region.

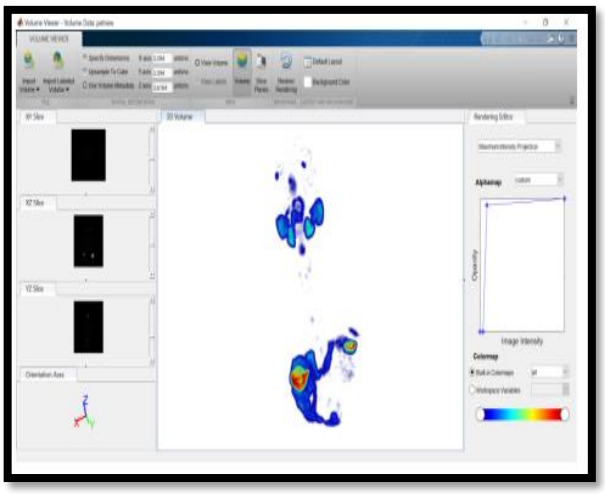

**Fig 3.15:** Reconstructed Image

GRAPHICAL USER INTERFACE

A GUI was also built to provide the user with immediate and visual feedback with details regarding classification results from the SVM model, statistical features of the image, and the various image processing steps.

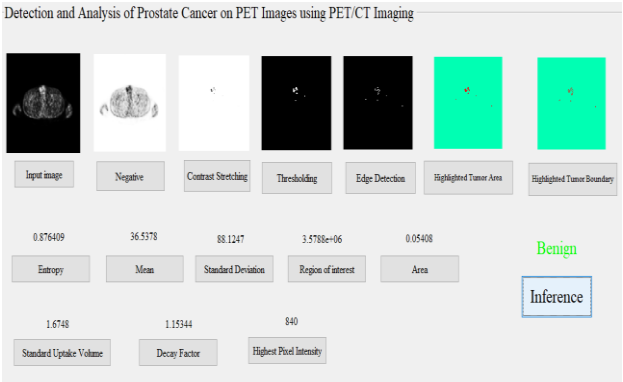


**Fig 3.16:** GUI representation

## 4. Discussion and Conclusion

It is seen that Standard Uptake Value (SUV) gives the measurement of the tracer uptake in a lesion normalized to a distribution volume, which has been the only and predominantly considered factor to determine if a region is malignant or benign [27].

Understanding of Multi-modal imaging in evaluation of tumor response to therapy and accurately identifying the diseased region with high resolution is considered. Clinical utility of 18F Choline instead of Fluoro-deoxy-glucose (FDG) for imaging the metastasis staging of high-risk prostate cancer was observed.

Segmentation methods used to obtain the ROI were Otsu's thresholding, graph-based co-segmentation, active contour methods which required manual specification of the threshold value through the histogram analysis.

Hence the need for automated segmentation and classification of the tumor region based on other useful parameters along with the SUV was observed for faster and accurate classification.

We were able to segment the cancer cells (region of interest) and extract features from the PET/CT images. A difference was seen during the statistical analysis of benign and malignant tumours which could help in further classification. Certain features like SUV could be relied on while classifying. Various methods of classification was carried like back propagation, SVM and CNN which resulted in accuracies of above 85%. 3D reconstruction of the processed image slices was implemented to assist in visualization for the physicians. A graphical user interface was also developed to enable a simpler user experience while using the solution.

The boundary of the tumour was automatically detected and drawn. The GUI is also able to provide the classification result that the physician can reference. The comparison of the three methods clearly shows that the Back Propagation method and the SVM method results in accuracy value better than CNN as the data set is relatively small. The experiment when implemented on open source data set having a size of >80 images, the CNN model proved to have higher accuracy. Hence one can infer that classification is good in SVM model and the Accuracy is good in CNN model when the procees was implemented on large datasets. Hence this work resulted in:

- Understanding the importance of PET imaging in identifying prostrate cancer. Many image processing methods and techniques that have been implemented and we have attempted to give an insight and a probable way of providing a Computer Aided Diagnostic Tool using CNN approach.
- In addition, this work has explored the qualitative approach in analysis of the methods implemented.

## 5. Future Scope

With a bigger dataset, a more robust and accurate classification model can be built. The three methods of classification and the level of accuracy that each method could offer is attempted in this paper can be expanded with a larger dataset. Depending on the accuracies of each method, one could be chosen and perfected. The larger multicentric study as well as correlation of the histopathological data for each image could enhance the use of assistive analysis as a part of radiological information systems in healthcare sector.

## 6.Acknowledgements

Our sincere thanks to the support of Dr.Prashanth, HCG Comprehensive Cancer Care Hospital for providing the domain support and do a enable us to run a sample trail on the dataset.

## References

[1] Hassanipour, S., Delam, H., Arab-Zozani, M., Abdzadeh, E., Hosseini, S. A., Nikbakht, H. A., Malakoutikhah, M., Ashoobi, M. T., Fathalipour, M., Salehiniya, H., &Riahi, S. (2020). Survival Rate of Prostate Cancer in Asian Countries: A Systematic Review and Meta-Analysis. Annals of global health, 86(1), 2. https://doi.org/10.5334/aogh.2607

[2] Hossein Jadvar."Molecular Imaging of Prostate Cancer: PET Radiotracers , Nuclear Medicine and Molecular Imaging • Review , http://doi.org/10.2214/AJR.12.8816

[3] Unterrainer, M., Eze, C., Ilhan, H. et al." Recent advances of PET imaging in clinical radiation oncology." Radiat Oncol 15, 88 (2020). http://doi.org/10.1186/s13014-020-01519-1

[4] Matteo Bauckneht, Francesco Bertagna, Maria Isabella Donegani, RexhepDurmo, Alberto Miceli, Vincenzo De Biasi, Riccardo Laudicella, Giuseppe Fornarini, Alfredo Berruti, Sergio Baldari, AnnibaleVersari, Raffaele Giubbini, GianmarioSambuceti, Silvia Morbelli& Domenico Albano, "The prognostic power of 18F-FDG PET/CT extends to estimating systemic treatment response duration in metastatic castration-resistant prostate cancer (mCRPC) patients." Prostate Cancer Prostatic Dis (2021). https://doi.org/10.1038/s41391-021-00391-8

[5] Steven Korevaar, Ruwan Tennakoon, Mark Page, Peter Brotchie, John Thangarajah, Cosmin Florescu, Tom Sutherland, Ning Mao Kam & Alireza Bab-Hadiasharl." Incidental detection of prostate cancer with computed tomography scans." Sci Rep 11, 7956 (2021), http://doi.org/10.1038/s41598-021-86972-y

[6] Nickols N, Anand A, Johnsson K, Brynolfsson J, Borrelli P, Juarez J, Parikh N, Jafari L, Eiber M, Rettig MB."aPROMISE: A Novel Automated-PROMISE platform to Standardize Evaluation of Tumor Burden in $^{18}$F-DCFPyL (PSMA) images of Veterans with Prostate Cancer." J Nucl Med. 2021, http://doi.org/10.2967/jnumed.120.261863

[7] Ntakolia, Charis &Diamantis, Dimitris &Papandrianos, Nikolaos &Moustakidis, Serafeim&Papageorgiou, Elpiniki. (2020). "A Lightweight Convolutional Neural Network Architecture Applied for Bone Metastasis Classification in Nuclear Medicine: A Case Study on Prostate Cancer Patients." Healthcare.8(4)493. http://doi.org/10.3390/healthcare8040493.

[8] Aphinives, C., Aphinives, P. "Artificial intelligence development for detecting prostate cancer in MRI." Egypt J RadiolNucl Med 52, 87 (2021),http://doi.org/10.1186/s43055-021-00467-4

[9] Baratto, L., Duan, H., Laudicella, R. et al. Physiological $^{68}$Ga-RM2 uptake in patients with biochemically recurrent prostate cancer: an atlas of semi-quantitative measurements. Eur J Nucl Med Mol Imaging 47, 115–122 (2020). https://doi.org/10.1007/s00259-019-04503-4

[10] Morand, G. B., Vital, D. G., Kudura, K., Werner, J., Stoeckli, S. J., Huber, G. F., &Huellner, M. W. (2018). "Maximum Standardized Uptake Value ($SUV_{max}$) of Primary Tumor Predicts Occult Neck Metastasis in Oral Cancer. "Scientific reports, 8(1), 11817. doi:10.1038/s41598-018-30111-7

[11] MR. Mohana Priya, P. Venkatesan, "An efficient image segmentation and classification of lung lesions in pet and CT image fusion using DTWT incorporated SVM, Microprocessors and Microsystems, Volume 82, 2021, 103958, ISSN 0141-9331, https://doi.org/10.1016/j.micpro.2021.103958.

[12] Van Booven J, Kuchakulla M, Pai R, Frech FS, Ramasahayam R, Reddy P, Parmar M, Ramasamy R, Arora H. "A Systematic Review of Artificial Intelligence in Prostate Cancer." Res Rep Urol. 2021;13:31-, 39, http://doi.org/10.2147/RRU.S268596

[13] Young Sympascho, Metser Ur, Sistani Golmehr, Langer Deanna L., Bauman Glenn. "Establishing a Provincial Registry for Recurrent Prostate Cancer: Providing Access to PSMA PET/CT in Ontario, Canada" ,Front. Oncol., 02 August 2021 ,http://doi.org/10.3389/fonc.2021.722430

[14] Mi Jung Rho, Jihwan Park, HyongWoo Moon, Chanjung Lee, Sejin Nam, Dongbum Kim, Choung-Soo Kim, Seong Soo Jeon, Minyong Kang, Ji Youl Lee Dr. Answer AI for prostate cancer: Clinical outcome prediction model and service,Published:August 5, 2020,http://doi.org/10.1371/journal.pone.0236553

[15] Andrew Janowczyk , Patrick Leo ,Mark A Rubin, " Clinical deployment of AI for prostate cancer diagnosis" The Lancet Digital Health ,VOLUME 2, ISSUE 8, E383-E384,August, 2020 , http://doi.org/10.1016/S2589-7500(20)30163-1

[16] Peter Ström, Kimmo Kartasalo, Henrik Olsson,et.al, "Artificial intelligence for diagnosis and grading of prostate cancer in biopsies: a population-based, diagnostic study", The Lancet Oncology,vol 21, Issue 2, 2020, http://doi.org/10.1016/S1470-2045(19)30738-7.

[17] Harmon SA, Tuncer S, Sanford T, Choyke PL, Türkbey B. "Artificial intelligence at the intersection of pathology and radiology in prostate cancer." Diagn IntervRadiol. 2019;25(3):183-188. http://doi.org/10.5152/dir.2019.19125

[18] Hadavand, M. A., Mayer, D., Chen, W., Wnorowski, A., & Siddiqui, M. M. (2020). Role of metabolic imaging in diagnosis of primary, metastatic, and recurrent prostate cancer. Current opinion in oncology, 32(3), 223–231. https://doi.org/10.1097/CCO.0000000000000625

[19] Capobianco, N., Sibille, L., Chantadisai, M. et al. Whole-body uptake classification and prostate cancer staging in $^{68}$Ga-PSMA-11 PET/CT using dual-tracer learning. Eur J Nucl Med Mol Imaging (2021). https://doi.org/10.1007/s00259-021-05473-2

[20] Rachid Sammouda, Abdu Gumaei, Ali El-Zaart, "Intelligent Computer-Aided Prostate Cancer Diagnosis Systems: State-of-the-Art and Future Directions", Mathematical Problems in Engineering, vol. 2021, Ar.ID 9955174, 17 pages, 2021,http://doi.org/10.1155/2021/9955174

[21] Detection of Prostate Cancer Using Deep Learning Framework Abhishek Patel , Sanjay Kumar Singh and Aditya Khamparia. ICCRDA 2020 IOP Conf. Series: Materials Science and Engineering 1022 (2021) doi:10.1088/1757-899X/1022/1/012073

[22] Bayerschmidt, S.; Uprimny, C.; Kroiss, A.S.; Fritz, J.; Nilica, B.; Svirydenka, H.; Decristoforo, C.; von Guggenberg, E.; Horninger, W.; Virgolini, I.J. Comparison of Early Imaging and Imaging 60 min Post-Injection after Forced Diuresis with Furosemide in the Assessment of Local Recurrence in Prostate Cancer Patients with Biochemical Recurrence Referred for 68Ga-PSMA-11 PET/CT. Diagnostics 2021, 11, 1191, http://doi.org/10.3390/diagnostics11071191

[23] Walter Jentzen, Lutz Freudenberg, Ernst G. Eising, Melanie Heinze, Wolfgang Brandau, Andreas Bockisch , "Segmentation of PET Volumes by Iterative Image Thresholding", Journal of Nuclear Medicine Jan 2007, 48 (1) 108-114 . Rachid Sammouda, Abdu Gumaei, Ali El-Zaart, "Intelligent Computer-Aided Prostate Cancer Diagnosis Systems: State-of-the-Art and Future Directions", MathematicalProblems in Engineering, vol. 2021, Article ID 9955174,17 pages, 2021 ,https://doi.org/10.1155/2021/9955174

[24] Abdelmaksoud, I.R.; Shalaby, A.; Mahmoud, A.; Elmogy, M.; Aboelfetouh, A.; Abou El-Ghar, M.; El-Melegy, M.; Alghamdi, N.S.; El-Baz, A. Precise Identification of Prostate Cancer from DWI Using Transfer Learning. Sensors 2021, 21, 3664. https://doi.org/10.3390/ s21113664

[25] EldadRubinstein, MosheSalhov, MeitalNidam-Leshem et.al. "Unsupervised tumor detection in Dynamic PET/CT imaging of the prostate," Medical Image Analysis , Volume 55, July 2019,

Pages 27-40 , http://doi.org/10.1016/j.media.2019.04.001

[26] Hartenstein, A., Lübbe, F., Baur, A.D.J. et al. Prostate Cancer Nodal Staging: Using Deep Learning to Predict $^{68}$Ga-PSMA-Positivity from CT Imaging Alone. Sci Rep **10,** 3398 (2020). https://doi.org/10.1038/s41598-020-60311-z]

[27] Ayyad, S.M.; Shehata, M.; Shalaby, A.; Abou El-Ghar, M.; Ghazal, M.; El-Melegy, M.; Abdel-Hamid, N.B.; Labib, L.M.; Ali, H.A.; El-Baz, A. Role of AI and Histopathological Images in Detecting Prostate Cancer: A Survey. Sensors 2021, 21, 2586. https://doi.org/10.3390/s21082586

[28] https://wiki.cancerimagingarchive.net/display/Public/TCGA-PRAD

[29] Barwal, R. K. ., Raheja, N. ., Bhiyana, M. ., & Rani, D. . (2023). Machine Learning-Based Hybrid Recommendation (SVOF-KNN) Model For Breast Cancer Coimbra Dataset Diagnosis. International Journal on Recent and Innovation Trends in Computing and Communication, 11(1s), 23–42. https://doi.org/10.17762/ijritcc.v11i1s.5991

[30] Juan Garcia, Guðmundsdóttir Anna, Maria Jansen, Johansson Anna, Anna Wagner. Exploring Decision Trees and Random Forests for Decision Science Applications. Kuwait Journal of Machine Learning, 2(4). Retrieved from http://kuwaitjournals.com/index.php/kjml/article/view/211

[31] Gupta, R., Mane, M., Bhardwaj, S., Nandekar, U., Afaq, A., Dhabliya, D., Pandey, B.K. Use of artificial intelligence for image processing to aid digital forensics: Legislative challenges (2023) Handbook of Research on Thrust Technologies? Effect on Image Processing, pp. 433-447.